6 KUWAHARA, K.: Numerical study of flow past an inclined flat plate by an inviscid model. J. Phys. Soc. Japan **35** (1973), 5.
7 CLEMENTS, R. R.: An inviscid model of two-dimensional vortex shedding. J. Fluid Mech. **57** (1973), 2.
8 KIYA, M.; ARIE, M.: A contribution to an inviscid vortex shedding model for an inclined flat plate in uniform flow. J. Fluid Mech. **82** (1977), 2.

Address: Dipl.-Ing. P. LAMPART; Dr. Z. WIERCIŃSKI, Institute of Fluid-Flow Machinery, Polish Academy of Sciences, ul. Gen. J. Fiszera 14, 80-952 Gdańsk, Poland

3.5b SIMULATION VISKOSER STRÖMUNGEN

ZAMM · Z. angew. Math. Mech. **72** (1992) 5, T 369 – T 373 Akademie Verlag

KUDELA, H.

Study of the Motion of the Two-Dimensional Bubble by the Vortex Method

MSC (1980): 76E99 76B99 65C20

1. Introduction

One of the most important problems within the general area of pattern formation and bubbles (drops) mechanics concerns interface deformation. Special interest is paid to creating pattern formation of unstable flows [1]. In this paper our interest concerns the evolution of the two-dimensional bubble (closed interface) between two media with different densities under the action of gravity. When a heavy fluid is placed above a lighter one in the gravitational field Rayleigh-Taylor instability occurs. We adopted a relatively simple model: the fluid is assumed inviscid, immiscible and incompressible; its density is constant in a region separated by a close curved. The flow is two-dimensional and irrotational except at a sharp interface. Thus the interface can be regarded as a vortex sheet. Investigation of the interface motion can be expressed as an initial value problem and reduced to following a curve that moves with its own induced velocity. To simplify the numerical procedure we accepted the fact that density variations are small. This allowed us to significantly simplify the evolution equation for the vortex sheet strength and enabled us to avoid some problems related to nonlinearity of this equation [6]. Instead of Fredholm integral equation of second kind a simply differential equation had to be solved [4]. But the case still has practical interest e.g. in the study of motion of a thermal [2]. For the solution of the initial value problem we used the generalized vortex method described by BAKER, MARION, ORSZAG [4], [5] and BAKER [3]. It is known that the initial value problem for the vortex sheet is ill-posed in the Hadamard sense (at a finite time solution yields singularity [8], [6]). To regularize the problem KRASNY [7] modified the Biot-Savart formula by introducing δ^2-parameter and in such a way that the singular integrand is replaced by a smooth one. Although the introduction of δ^2 is a quite formal procedure KRASNY showed [7] that for the linearized δ^2-equation, short-wave-length behavior (its growth rate) is similar to the effect which the viscosity plays in the linearized Rayleigh-Taylor problem. For this reason, one can interpret the introduction of the δ^2-parameter as the trial to mimics of fluid viscositv.

2. The equation of motion

The interface was described parametrically $(x(e, t), y(e, t)$ where t is the time and e a real parameter $\in [0, 1]$ which was used also as a Lagrangian variable. At the initial instant the e value marks the point on the interface that allows following the motion of the interface. The initial shape of the bubble was described by ellipse equation $(x(e, 0) = a \cos(2\pi e)$, $y(e, 0) = b \sin(2\pi e))$ where a and b are large and small axes of the ellipse. Moreover the ellipse can be rotated on θ angle where θ is the angle between the large axis of the ellipse a and the horizontal axis x. So initial position and shape of bubble can be characterized by θ angle and the ratio $s = b/a$. Further, except the case of cylinder motion ($s = 1$), we presented results only for the evolution of the ellipse with $s = 1/3$, $a = 1$ and the different θ angle. By virtue of the Biot-Savart formula and Bussinesq approximation δ^2-equations for velocity and equation for the evolution of the vortex sheet

strength are:

$$\frac{\partial x}{\partial t} = -\frac{1}{2\pi}\int_0^1 \frac{\gamma(e', t)\,(y(e, t) - y(e', t))}{r^2 + \delta^2}\,\mathrm{d}e', \tag{1}$$

$$\frac{\partial y}{\partial t} = \frac{1}{2\pi}\int_0^1 \frac{\gamma(e', t)\,(x(e, t) - x(e', t))}{r^2 + \delta^2}\,\mathrm{d}e', \tag{2}$$

$$\frac{\partial \gamma}{\partial t} = 2\frac{\partial y}{\partial e}, \tag{3}$$

where $r^2 = (x(e, t) - x(e', t))^2 + (y(e, t) - y(e', t))^2$, $\gamma(e, t)$ is the sheet strength for the Lagrangian variable [5]. The units used in (1)–(3) are such that the length is scaled by a and time by $(a/Ag)^{1/2}$ where $A = (\varrho_1 - \varrho_2)/(\varrho_1 + \varrho_2)$ is the so-called Atwood number and ϱ_1 is the density of the ambient fluid, ϱ_2 is the density of the fluid in the bubble. In the Boussinesq limit $A \to 0$, $g \to \infty$ such that Ag remains constant (g-acceleration due to gravity). The numerical procedure is as follows: for $x(e, t)$, $y(e, t)$, $\gamma(e, t)$ (initially $\gamma(e, 0) = 0$), the interface is marched forward using (1), (2) and next also $\gamma(e, t)$ is marched forward from (3). The Adam-Multon predictor corrector scheme of fourth-order was used for solution of (1), (2), (3). To start calculations the Runge-Kutta (RKF45) algorithm was used. The derivative with respect to the Lagrangian variable e was calculated by cubic spline. Integrals were evaluated using trapezoidal rules on an alternate set of points [3]. Calculation was carried out on an IBM PC-386 computer in double precision arithmetic using RMFORTRAN. For checking accuracy the two invariant of the motion was monitored: mass of the bubble and mass flux though interface. When the relative error was greater then 0.05 the calculation was stopped. The time step and the number of vortices were chosen experimentally and it was accepted $\triangle t = 0.005$, and $N = 300$.

3. Numerical results

3.1 Motion of cylindrical bubble

The vortex study of this case has already been done by ANDERSON (but by another vortex method) [2] and MENG, THOMSON [9]. We repeated the calculation for rise of a buoyant cylinder (or a thermal) to gain the understanding of δ^2 influence. Fig. 1 shows the sequence of the solutions for evolving the cylindrical bubble for $\delta^2 = 0.01$. The creation of two vortices

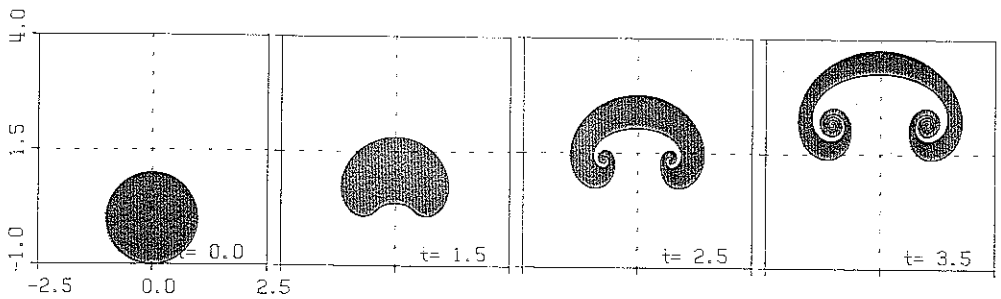

Fig. 1. Successive stages in the evolution of cylindrical bubble with $\delta^2 = 0.01$. The time is indicated on the right of each frame

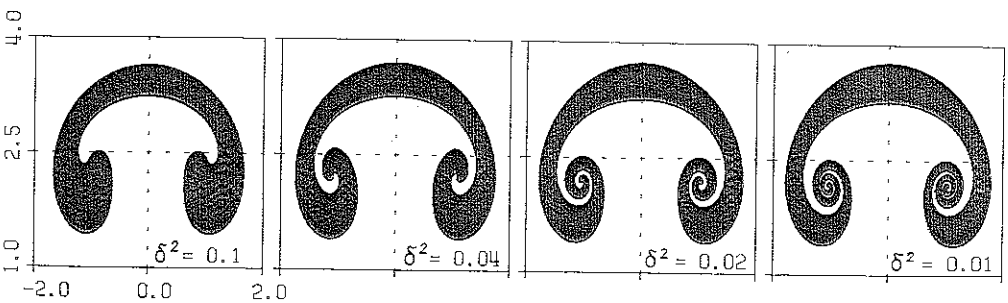

Fig. 2. Effect of δ^2 value. Interface at $t = 3.5$, δ^2 value as shown

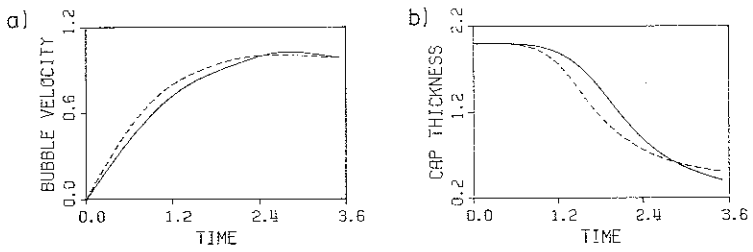

Fig. 3. a) Velocity of upper point of the bubble vs time, b) cap thickness vs time. The solid line $\delta^2 = 0.1$, dash line $\delta^2 = 0.01$

with spiral structure on both sides of the vertical axis of symmetry is clearly visible. The rate of change of the total vorticity in one half of the curve is measured by the thickness $\triangle y$ of the cap on the axis of symmetry (integration of (3) with respect to e in the interval $[0, 0.5]$ gives $\dfrac{\partial}{\partial t}\displaystyle\int_0^{0.5} \gamma = 2\triangle y$). To illustrate the influence of the value of δ^2 in Fig. 2 we showed the solutions with different δ^2 in the same time. One can see that while large scales of bubble suffer only slight changes the spiral structure becomes more and more complicated (has more turns) when δ^2 is decreased. Fig. 3a presents the velocity of the upper point of the bubble (on the symmetry axis) vs. time and in Fig. 3b the thickness of the cap vs. time for $\delta^2 = 0.1$ and 0.01 (graphs for $\delta^2 = 0.04$ and 0.02 laid between this two curves). Fig. 3a suggests that the limit for velocity of the upper point of the bubble exists independently from δ^2 value. Greater value of the δ^2 (more "viscous" fluids) causes slower raising of velocity (Fig. 3 a) and drops the rate of total change vorticity more quickly (Fig. 3b).

3.2 Motion of elliptical bubble

Fig. 4 shows the evolution of a bubble for $\delta^2 = 0.02$, and $\theta = 60°$. At first one may be surprised that a tail structure has developed. The tail starts to come out at the point where $\partial y/\partial e = 0$ so from (3) we see that the production of the vortex

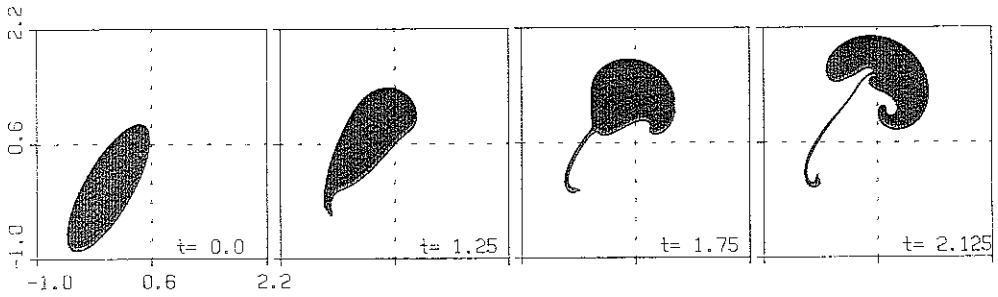

Fig. 4. Successive stages in the evolution of elliptical bubble with $\theta = 60°$, $\delta^2 = 0.02$. The time is indicated on the right of each frame

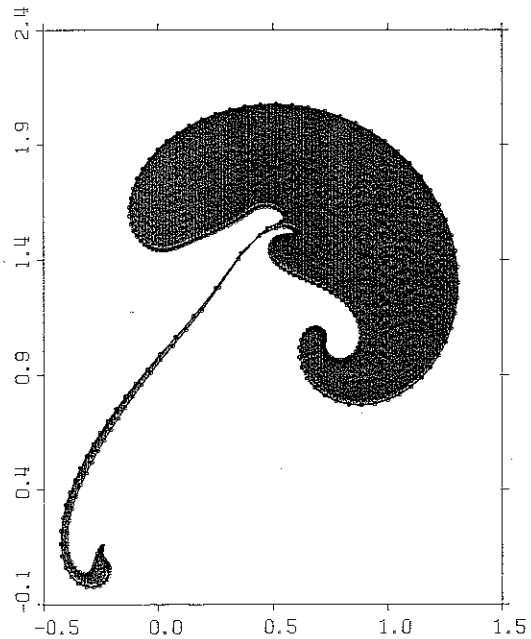

Fig. 5. Close-up of the frame for $t = 2.125$ from Figure 4. The points on the interface indicate the positions of markers moving with Lagrangian velocity

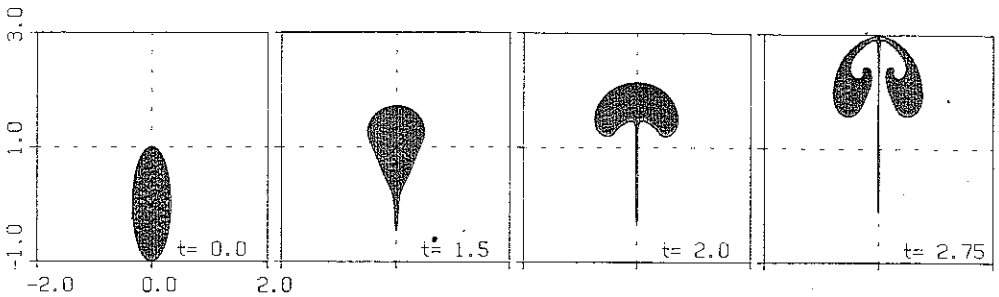

Fig. 6. Successive stages in the evolution of elliptical bubble with $\theta = 90°$, $\delta^2 = 0.04$. The time is indicated on the right of each frame

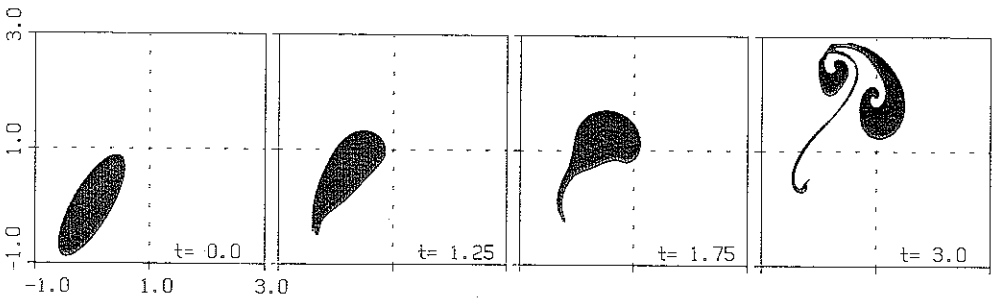

Fig. 7. Successive stages in the evolution of elliptical bubble with $\theta = 60°$, $\delta^2 = 0.04$

strength has an extremum. The tail (fluid thread) is stretched and its thickness at some point goes to zero (at this point probably the tail will be separated from the bubble). Ambient fluid enter into the bubble near the base tail where the interface begun to develop in complex, fine structure. This fine structure around the base of the tail did not appear when the δ^2 parameter was increased ($\delta^2 = 0.04$ see Fig. 7). The tail ends in a spike. The upper part of the bubble tends to form a circular shape. A close-up frame for $t = 2.125$ from Fig. 4 was shown in Fig. 5. The point on the interface indicates the positions of the vortices. In Fig. 6, 7, 8, 9 we presented the evolution of the bubble for $\theta = 90°$, 60°, 45°, 30° respectively ($s = 1/3$) and $\delta^2 = 0.04$. In all cases we can see the same similarities but we can see also some differences especially in the evolution of the tail. In Fig. 9 at final stage of the evolution we have only two ends of the bubble and the tail is not ended with spike (for $\theta = 0$, $s = 0.333$ the evolution goes similar to that in Fig. 1).

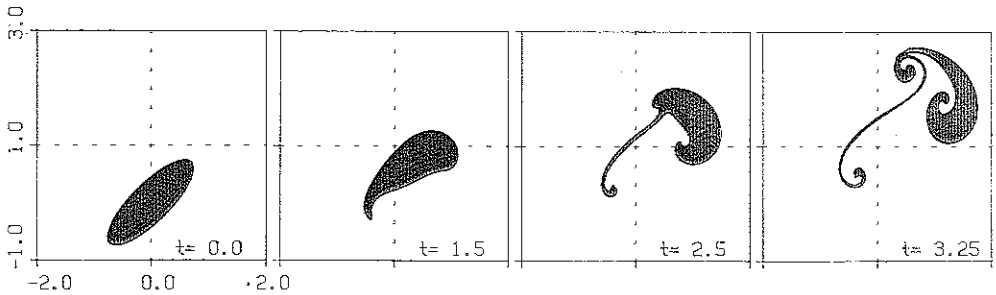

Fig. 8. Successive stages in the evolution of elliptical bubble with $\theta = 45°$, $\delta^2 = 0.04$

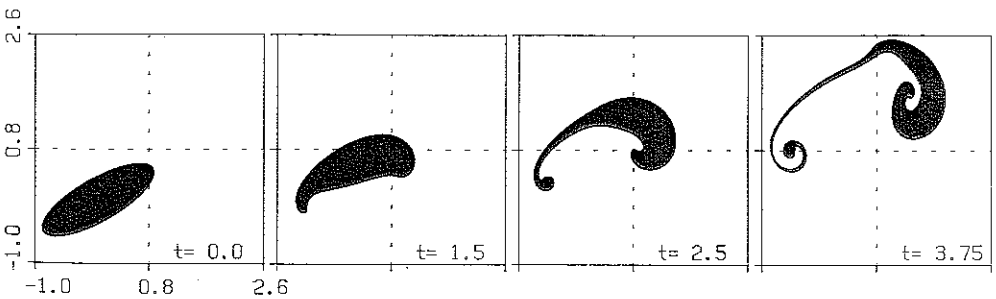

Fig. 9. Successive stages in the evolution of elliptical bubble with $\theta = 30°$, $\delta^2 = 0.04$

4. Closing remarks

As it is suspected, the evolution of the bubble in an unstable flow (Rayleigh-Taylor instability) is sensitive to initial conditions (shape). Development of tails, spikes and whirls are typical entities which can be noticed in the evolutions of the forms in unstable flows [1]. Despite of our two-dimensional flows the quantitative results are similar to those presented by POZRIKIDIS [10] for spherical drops. The δ^2-parameter mimics the viscosity of the fluids: greater (more "viscous") value of δ^2 prevent the evolution of very complicated shapes of the interface and change timescale of deformations. It is clear that the evolution of the bubble will be sensitive to b/a ratio. When this ratio is large enough ($b/a > 0.5$) the evolution will resemble the one Fig. 1 or 9.

References

1 AREF, H.: Finger, bubble, tendril, spike. Fluid Dyn. Trans., Polish Sci. Publisher, Warsaw **13** (1987), 25–54.
2 ANDERSON, C.: A vortex method for flows with slight density variations. J. Comput. Phys. **61** (1985), 417–444.
3 BAKER, G. R.: Generalized vortex methods for free-surface flows. Proc. Wave on Fluid Interface, Academic Press 1983, pp. 53–81.
4 BAKER, G. R.; MEIRON, D. I.; ORSZAG, S. A. : Vortex simulation of the Rayleigh-Taylor instability. Phys. Fluids. **23** (1982), 1485–1490.
5 BAKER, G. R.; MEIRON, D. I.; ORSZAG, S. A.: Generalized vortex methods for free-surface flow problems. J. Fluid Mech. **123** (1982), 477–501.
6 KUDELA, H.: The influence of surface-tension effects on using vortex method in the study of Rayleigh-Taylor instability. Notes on numerical fluid mechanics **29** (1990), 273–282 (Ed. WESSELING, P., Vieweg).
7 KRASNY, R.: Desingularization of periodic vortex sheet roll-up. J. Comput. Phys. **65** (1986), 123–155.
8 KRASNY, R.: A study of singularity formation in a vortex sheet by the point-vortex approximation. J. Fluid Mech. **167** (1986), 65–93.
9 MENG, J. C. S.; THOMSON, J. A. L.: Numerical studies of some nonlinear hydrodynamic problems by discrete vortex element method. J. Fluid Mech. **84** (1978), 433–453.
10 POZRIKIDIS, S. C.: The instability of a moving viscous drop. J. Fluid Mech. **210** (1990), 1–21.

Address: Dr. HENRYK KUDELA, Technical University of Wrocław, Institute of Heat Engineering and Fluid Mechanics, 50-370 Wrocław, Wybrzeże, Wyspiańskiego 27, Poland

ZAMM · Z. angew. Math. Mech. **72** (1992) 5, T 373–T 377 Akademie Verlag

PERKTOLD, K.; HILBERT, D.; SIEKMANN, J.

Numerische Untersuchung der pulsatilen Strömung eines nicht-Newtonschen Fluides in einem elastischen Rohr

MSC (1980): 76A05

Untersucht wird die Wechselwirkung der elastisch deformierbaren Wand und der pulsatilen Strömung in einem Rohr mit endlicher Länge. Die durchgeführten Studien sind motiviert durch die Strömungsanalyse in Arterien und zeigen den Einfluß der Wandelastizität auf die Strömungsgeschwindigkeit und auf die Deformation der Wand eines rohrförmigen Arterienabschnittes. In der zugrunde gelegten mathematischen Beschreibung wird das Hauptgewicht auf die Strömung gelegt; die Erfassung der deformierbaren Wand erfolgt durch ein einfaches idealisiertes Modell. Der Vergleich der Ergebnisse mit theoretischen und experimentellen Resultaten zeigt gute Übereinstimmung und rechtfertigt die vereinfachenden Annahmen für die Wandbewegung bei der lokalen Strömungsanalyse in Arterien. Als strömendes Medium wird ein inkompressibles Fluid mit Scherverdünnungseigenschaften und Yieldspannung angenommen. Die vereinfachte rheologische Beschreibung von Blut erfolgt mit der Casson-Beziehung auf der Basis von Meßdaten für eine mit zwei Hertz oszillierende Strömung [4].

Die betrachtete Strömung wird durch die Navier-Stokes Gleichungen für inkompressible, verallgemeinerte Newtonsche Fluide beschrieben. In der Spannungs-Divergenz-Formulierung gilt für den rotationssymmetrischen Fall (r, θ, z)

$$\varrho\left(\frac{\partial u}{\partial t} + u\frac{\partial u}{\partial r} + v\frac{\partial u}{\partial z}\right) + \frac{\partial p}{\partial r} - \frac{\partial \tau_{rr}}{\partial r} - \frac{\partial \tau_{rz}}{\partial z} - \frac{1}{r}(\tau_{rr} - \tau_{\theta\theta}) = 0\,,$$
$$\varrho\left(\frac{\partial v}{\partial t} + u\frac{\partial v}{\partial r} + v\frac{\partial v}{\partial z}\right) + \frac{\partial p}{\partial z} - \frac{\partial \tau_{rz}}{\partial r} - \frac{1}{r}\tau_{rz} - \frac{\partial \tau_{zz}}{\partial z} = 0\,, \tag{1}$$

$$\frac{\partial u}{\partial r} + \frac{u}{r} + \frac{\partial v}{\partial z} = 0\,. \tag{2}$$

Die in (1) auftretenden Extra-Spannungskomponenten sind durch das konstitutive Gesetz erklärt:

$$\tau_{rr} = 2\mu(DII)\frac{\partial u}{\partial r}, \qquad \tau_{zz} = 2\mu(DII)\frac{\partial v}{\partial z},$$
$$\tau_{\theta\theta} = 2\mu(DII)\frac{u}{r}, \qquad \tau_{rz} = \mu(DII)\left(\frac{\partial u}{\partial z} + \frac{\partial v}{\partial r}\right). \tag{3}$$

Die Viskosität $\mu(DII)$ ist eine Funktion der zweiten Invarianten des Verzerrungsratentensors

$$DII = \frac{1}{2}\left[\left(\frac{\partial u}{\partial r}\right)^2 + \left(\frac{u}{r}\right)^2 + \left(\frac{\partial v}{\partial z}\right)^2 + \frac{1}{2}\left(\frac{\partial u}{\partial z} + \frac{\partial v}{\partial r}\right)^2\right]. \tag{4}$$

Mit (4) folgt für die Scherrate $\dot{\gamma}$ einer einfachen Scherströmung $\dot{\gamma} = 2\sqrt{DII}$.

Für die Bewegung der elastischen Wand gilt unter der Voraussetzung eines dünnwandigen Rohres mit kleiner Deformation und großer Pulswellengeschwindigkeit (in Arterien ca. 10 m/sec)

$$\varrho_w \frac{\partial^2 w_r}{\partial t^2} = -\frac{E}{1-\nu^2}\left(\frac{w_r}{r_0^2} + \frac{\nu}{r_0}\frac{\partial w_z}{\partial z}\right) + f_r',$$
$$\varrho_w \frac{\partial^2 w_z}{\partial t^2} = \frac{E}{1-\nu^2}\left(\frac{\nu}{r_0}\frac{\partial w_r}{\partial z} + \frac{\partial^2 w_z}{\partial z^2}\right) + f_z'. \tag{5}$$

Die Koppelung des Fluids mit der elastischen Wand erfolgt über die Körperkräfte f_r' und f_z'. Im Übergang vom Fluid zur Wand tritt die Gleichheit der Geschwindigkeit und der Oberflächenkräfte auf. Mit τ_{rr} und τ_{rz} nach (3) ist

$$f_r' = \frac{1}{h}(p - \tau_{rr}) \qquad f_z' = -\frac{1}{h}\tau_{rz}. \tag{6}$$

Die durch (5) mit (6) bestimmte Wandbewegung wird durch die Annahme, daß nur Deformation in radialer Richtung auftritt ($w_z = 0$), stark vereinfacht. Für die Wandbewegung gilt damit

$$m\frac{\partial^2 w_r}{\partial t^2} = p_w - \alpha\frac{r - r_0}{r_0}, \qquad \alpha = \frac{Eh_0}{r_0}. \tag{7}$$

Diese Idealisierung bringt zum Ausdruck, daß die Rohrwand aus ringförmigen Segmenten besteht, zwischen denen keine Kraft und damit keine longitudinale Dehnung auftritt [2]. Diese Annahme findet eine gewisse Rechtfertigung in den Ergebnissen nach [8]. Auch die Resultate in [3] unterstützen diese Modellannahmen.

Iteratives Lösungsverfahren

Die Lösung für einen Zeitschritt wird iterativ durch die Folge $(r^0, u_w^0, u^0, v^0, p^0)$, $(r^1, u_w^1, u^1, v^1, p^1)$, ... angenähert. Die Werte $r^0 = \bar{r}$, $u_w^0 = \bar{u}_w$, $u^0 = \bar{u}$, $v^0 = \bar{v}$, $p^0 = \bar{p}$ bezeichnen Endwerte für den vorherigen Zeitschritt.

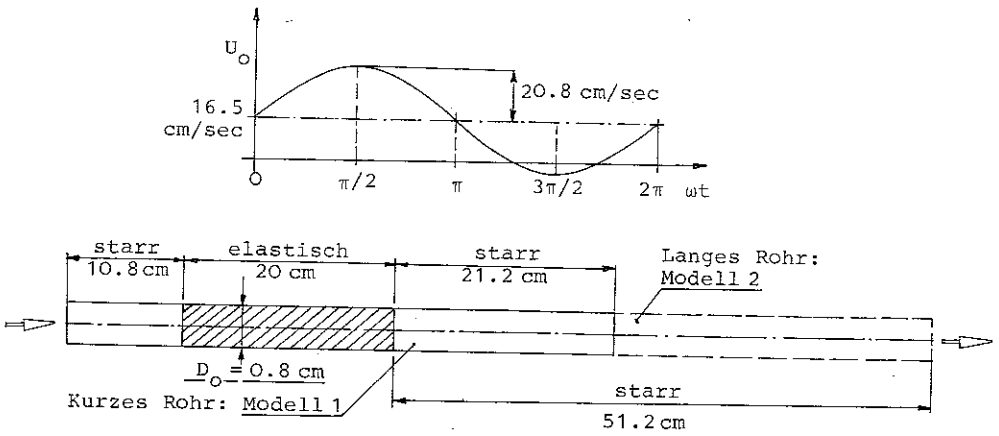

Abb. 1. Rohrmodell und Geschwindigkeitspuls im Eintritt; Rohrinnendurchmesser $D_0 = 0{,}8$ cm, Wanddicke $h_0 = 0{,}1$ cm; Gesamtlänge: Modell 1 $L = 52$ cm, Modell 2 $L = 82$ cm. Einströmung: Mittlere Reynoldszahl $Re = 600$, Frequenz des Pulses $f = 1{,}4$ Hz.